Evaluation of image reconstruction algorithms encompassing Time-Of-Flight and Point Spread Function modelling for quantitative cardiac PET: Phantom studies

L. Presotto,[a,b] L. Gianolli,[a] M. C. Gilardi,[b] and V. Bettinardi[a]

[a] Nuclear Medicine Unit, IRCCS Ospedale San Raffaele, Milan, Italy
[b] Institute of Molecular Bioimaging and Physiology, National Research Council, Segrate, Italy

Received Jul 21, 2014; accepted Oct 14, 2014
doi:10.1007/s12350-014-0023-1

Background. **To perform kinetic modelling quantification, PET dynamic data must be acquired in short frames, where different critical conditions are met. The accuracy of reconstructed images influences quantification. The added value of Time-Of-Flight (TOF) and Point Spread Function (PSF) in cardiac image reconstruction was assessed.**

Methods. **A static phantom was used to simulate two extreme conditions: (i) the bolus passage and (ii) the steady uptake. Various count statistics and independent noise realisations were considered. A moving phantom filled with two different radionuclides was used to simulate: (i) a great range of contrasts and (ii) the cardio/respiratory motion. Analytical and iterative reconstruction (IR) algorithms also encompassing TOF and PSF modelling were evaluated.**

Results. **Both analytic and IR algorithms provided good results in all the evaluated conditions. The amount of bias introduced by IR was found to be limited. TOF allowed faster convergence and lower noise levels. PSF achieved near full myocardial activity recovery in static conditions. Motion degraded performances, but the addition of both TOF and PSF maintained the best overall behaviour.**

Conclusions. **IR accounting for TOF and PSF can be recommended for the quantification of dynamic cardiac PET studies as they improve the results compared to analytic and standard IR. (J Nucl Cardiol 2015;22:351–63.)**

Key Words: Partial volume effect • image reconstruction • myocardial perfusion imaging: PET • image processing

INTRODUCTION

Myocardial blood flow (MBF) has been shown to be an important prognostic[1] and diagnostic[2] parameter for cardiovascular disease evaluation. It can be quantified with positron emission tomography (PET) and myocardial perfusion radiotracers such as ^{15}O-water, ^{13}N-ammonia and ^{82}Rb.[3] New ^{18}F-tracers are also currently being evaluated, to expand the clinical use of this methodology.[4] Absolute MBF quantification can be performed acquiring a dynamic scan and analysing the tracer concentration in the blood and in the myocardial tissue over time by means of kinetic models which estimate the rate constants representative of the underlying physiological processes.[3] The goodness of the estimated parameters depends on the accuracy of acquisition and reconstruction of PET images.

A dynamic perfusion PET study is constituted by multiple frames, each with different characteristics. Initial frames, corresponding to the arrival of the tracer bolus in the heart, are characterised by a very high activity and, therefore, by high count rates, high dead-time levels and high fractions of random coincidences. Furthermore, the fast kinetics of perfusion tracers in the initial passage in the heart, require the use of short

Reprint requests: L. Presotto, Nuclear Medicine Department, San Raffaele Hospital, Milan, Italy; *presotto.luca@hsr.it*
1071-3581/$34.00

acquisition frames (e.g., ~10 seconds) resulting in a poor count statistics and, consequently, in a high noise level in the reconstructed PET images. Conversely, in later frames the activity extracted from the blood is retained in the myocardial tissue and, at least for the tracers that are metabolised with an irreversible uptake, a steady state is reached. In such condition, the activity in the field of view (FOV) is significantly reduced and therefore count rates, dead-time and random coincidences are much lower. Furthermore, longer acquisition frames (20 seconds or more) can be used to increase the count statistics for a better image quality.

Quantitative cardiac PET images are traditionally reconstructed using analytical techniques, like filtered-back-projection (FBP), mainly for their linearity.[5] A different option is to use iterative statistical algorithms, like the maximum likelihood expectation maximisation (MLEM) and its accelerated implementation, the ordered subset expectation maximisation (OSEM).[6]

Iterative algorithms currently represent the standard in qualitative oncologic imaging, thanks to their favourable noise properties, higher contrast and better spatial resolution respect to the analytical ones.[7-9] In dynamic cardiac PET studies, however, they have not been systematically introduced yet because of their intrinsic nonlinearity and for the tendency to generate a positive bias in cold regions, in particular when the statistics is poor.[10,11]

Iterative algorithms for oncologic PET have been recently largely improved. Modelling of the Time-Of-Flight (TOF) information, Point Spread Function (PSF) of the PET tomograph and more sophisticated implementations of all the corrections have been introduced. In particular, TOF information has been shown to improve the signal to noise ratio,[12] to speed up convergence[13] and to make the reconstruction more robust vs imprecise corrections.[14] The PSF modelling recovers the spatial resolution degradation and thus is able to reduce the associated partial volume effect (PVE), that is particularly relevant for structures with dimension <2.5 the full with at half of the maximum (FWHM) of the PET system.[15]

The efficacy of OSEM with PSF modelling in cardiac ^{18}F-FDG studies was investigated by Le Meunier et al[16] who found that it improves contrast and defects definition while reducing image noise. Another study[11] also found that PSF reduces inter-voxel variance, as well as the amount of bias in low-statistics frames. Recently, Armstrong et al[17] compared the results obtained in ^{82}Rb MBF quantification between OSEM reconstructions and a reconstruction protocol encompassing both TOF and PSF modelling (TOFPSF). In this work, only a single setting of parameters (21 subsets, 2 iterations and 6.5 mm post-filtering) was evaluated. The results showed an increase (~+10%) of the quantified MBF for TOFPSF reconstructions. In particular, it was found that the area under the curve of the input function (IF) was lower in the TOFPSF by up to 10%, but it was not reported whether this occurred because of differences in the first frames, when blood is the most radioactive compartment, or in later frames, when radioactivity is most in the heart tissue.

The aim of this study was to investigate the performances of such improved iterative reconstruction (IR) techniques in PET cardiac studies, under controlled conditions simulating different frames of a dynamic acquisition, i.e., over a wide range of count rates, activity distributions, statistics of acquisition and random coincidences rate. The ultimate objective was to assess if these algorithms could outperform the analytical ones and thus become the new standard for MBF quantification.

MATERIALS AND METHODS

PET Scanner

All the studies have been acquired on a Discovery 690 (D-690, General Electric Medical Systems - GEMS, Milwaukee, USA) PET/Computed Tomography (CT) system.[18] The D-690 operates in 3D mode with TOF technology. The available reconstruction algorithms are: analytical (3D-reprojection: RP) and iterative (3D-ordered subsets expectation maximisation: OSEM),[19] (GEMS name = VUE-point HD). With 3D-OSEM two further options can be activated: TOF information (GEMS name = VUE-point FX) and/or a spatial variant model of the D-690 PSF (GEMS name = Sharp-IR).[20]

Experimental Phantom Measurements

Two phantoms were used: an anthropomorphic thorax/heart static phantom and a moving phantom, shaped as the left ventricle. It can replicate both respiratory and cardiac motion. To simulate realistic conditions, the activity values used in the phantom compartments were based on average patient uptakes measured on clinical PET images, thus reproducing count rates and random coincidences fractions typically recorded in clinical studies.

Static Phantom Description

The thorax/heart phantom (model RH-2; Kyoto-Kagaku, Kyoto, Japan) (30 × 20 × 21 cm^3) consists of: (i) a body with two compartments simulating the lung, (ii) an insert for the liver, (iii) a rod to simulate the spine and (iv) a central compartment (mediastinum) with a heart model insert (Figure 1). The myocardium has a uniform wall thickness of 10 mm. To simulate perfusion or metabolic defects, small parallelepipeds of silicon or polystyrene can be inserted within the myocardium wall.

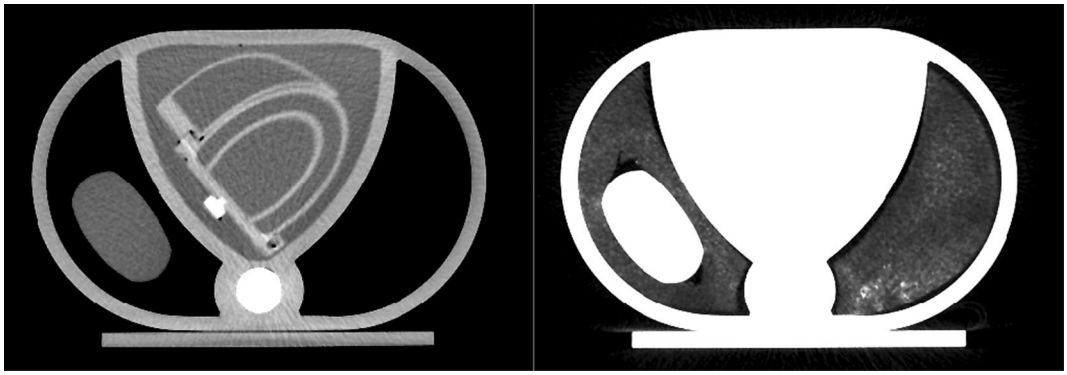

Figure 1. Thorax/heart phantom: A transaxial CT slice of the phantom is shown using two different *grey* window levels. The myocardium and the ''liver'' can be seen in the *left image* while in the *right one*, the porous structure of the lungs (spongy polymers) which can absorb a radiotracer, can be appreciated.

Static Phantom, First Configuration: Bolus Passage

This study aimed to simulate the first passage of the tracer bolus in the heart. This phase is characterised by high activities in the ventricles, a lower activity in the mediastinum and absent or very low activity in the myocardium.

The phantom was filled with a ^{18}F-FDG water solution with the following concentrations, calibrated to acquisition start time: 175 kBq·cc^{-1} in the right ventricle (RV), 133 kBq·cc^{-1} in the left ventricle (LV) and 70 kBq·cc^{-1} in the mediastinum. Activity retained in the lungs was about 7 kBq·cc^{-1}. In order to simulate out-of-FOV activity, two uniform phantoms (diameter = 20 cm, length = 20 cm), containing 37 MBq each, were positioned outside the FOV, in front of and behind the cardiac phantom.

In this configuration, a count rate of 2.4 Mcps was obtained, with estimated rates for true and random coincidences of 1.2 and 1.2 Mcps, respectively. The mean busy time of each block readout was 5.6%. These figures resemble those usually recorded in patient studies, with peak prompt coincidences count rates between 2 and 3.5 Mcps and block-busy time comprised between 5% and 7.5%.

The phantom was positioned in the FOV centre and an emission scan was acquired in list mode for 15 minutes. Ten frames of 2, 5 and 10 seconds and 6 frames of 20 and 40 seconds were extracted from the list-mode file. All the frames were independent, i.e., a single coincidence event was not used in more than one frame. Considering the short acquisition time compared to the ^{18}F half-life (110 minutes), each scan can be considered as an independent noise realisation of the same measure.

Targets of the experiment. The targets of this experiment were the assessment of: (i) the accuracy in the estimation of the LV activity as a function of different frame lengths; and (ii) the amount of positive bias in the cold myocardium region. For both targets, the associated standard deviation (STD) was evaluated on independent noise realisations of the same scan.

Static Phantom, Second Configuration: Steady State

The second study aimed to simulate the steady state of a tracer with an irreversible uptake, in which the activity is retained in the myocardial tissue.

The phantom was filled with a ^{18}F-FDG water solution with the following concentrations (reported activities are calculated at acquisition start): 54 kBq·cc^{-1} in the myocardium, 27 kBq·cc^{-1} in the liver, 8.6 kBq·cc^{-1} in the ventricles and 7.8 kBq·cc^{-1} in the mediastinum. About 4 kBq·cc^{-1} were retained in the lungs. Two infracted regions were simulated, covering the full myocardial thickness: one in the apical-lateral segment (15 × 22 × 10 mm^3) and one in the mid-anterior segment (30 × 15 × 10 mm^3). A prompt coincidences count rate of about 300 kcps was recorded, with an estimated 50 kcps count rate of random coincidences. These count rates are in line with those recorded in ^{13}N-ammonia patient studies, where they decrease from about 800 kcps 2 minutes after the injection to less than 150 kcps at the end of the 20 minutes scan.

As in the first study, the phantom was positioned in the centre of the FOV and an emission scan was acquired in list mode for 15 minutes. Ten independent noise realisations of 5, 15 and 45 seconds were generated from the list mode file.

Targets of the experiment. The targets of this study were to assess: (i) the accuracy in the estimation of the myocardial activity and its STD for the different noise realisations, and (ii) the quantitative ''detectability'' of the two simulated defects.

Moving Phantom Description

To account for the heart motion, a dynamic phantom was designed and built in our lab. It features both heart beating and respiratory motion.[21] It consists of two compartments simulating the LV, and the myocardial wall. The cardiac beating is achieved by rhythmically inflating the LV compartment. A microcontroller drives a gear-motor with a feedback from its position encoders. The motor acts on a piston that pushes a

water reservoir connected to the LV compartment. The expansion of the LV results in a stretching of the myocardium. The respiratory motion is simulated by a periodic translation (in the cranial-caudal direction) of a moving platform on top of which the LV phantom is positioned (Figure 2).

Moving Phantom Acquisition

To mimic dynamically varying activity contrasts, the myocardium and the LV compartments were filled with ^{18}F-FDG and ^{13}N-ammonia, respectively. Activity concentrations, at scan start, were 380 kBq·cc^{-1} in the ^{13}N compartment and 34 kBq·cc^{-1} in the ^{18}F one. Eight 5 minutes acquisitions with the phantom in motion (cardiac period: 59 bpm, respiratory period: 4 seconds) were interleaved with 8 acquisitions with the phantom turned off (static condition). Each acquisition was performed in list mode and lasted 5 minutes. The same framing scheme was used both for static and in-motion acquisitions, in order to reproduce the count statistics usually found in a dynamic scan study: the first scan was divided in 6 seconds frames; the four consecutive scans in 10 seconds frames, the last three scans in 25 seconds frames. Contrasts between the two compartments (myocardium: LV) ranged from 1:11 to 34:1 for the moving acquisition.

The prompt count rate at the beginning of the study was of 1,700 kcps, with an estimated random coincidences rate of 500 kcps. At the end of the acquisition, the count rate decreased to 150 kcps, with an estimated random coincidences rate of 2 kcps.

Targets of the experiment. The targets of this study were to assess: (i) the response of the different reconstruction algorithms over a wide range of contrasts (activity ratios) between LV and myocardium; and (ii) the effects of heart motion.

Attenuation Correction

All the PET studies were corrected for attenuation (AC) by using CT data. A helical CT scan (120 kV, 50 mA, 0.5 seconds rotation time, 3.75 mm slice thickness) was acquired in correspondence of each static PET study while a cine-CT (120 kV, 50 mA, 0.5 second rotation time, 5 mm slice thickness, 5 seconds cine duration) was performed when the phantom was in motion. Cine-CT scans were used to reduce the probability of mismatches between PET and CT data.[22,23] For each scan, the cine-CT images were processed to generate an average attenuation map to be used for the AC of the corresponding PET data.

Reconstruction Algorithms and Reconstruction Protocols

Emission data were reconstructed with the following algorithms:

(1) 3D-Reprojection[5] (RP),
(2) Fourier Rebinning (FORE)-TOF-FBP[24,25] (TOF-FBP),
(3) 3D-OSEM (OSEM),
(4) 3D-OSEM with TOF (TOF),
(5) 3D OSEM with PSF (PSF),
(6) 3D-OSEM with both TOF and PSF (TOFPSF).

The implementation details of the algorithms are reported in ''Appendix.'' Common reconstruction settings were: FOV diameter: 300 mm, matrix size: 256 × 256, voxel size: 1.17 × 1.17 × 3.27 mm^3. The analytical reconstructions were performed using a ramp filter. IRs were performed with 18 subsets and 10 iterations. Each iteration was saved and successively post-filtered with a transaxial Gaussian filter with 2 mm FWHM and a moving average filter with weights [1 6 1] in the axial direction. On the basis of the results obtained on the static phantom (see Results section), moving phantom data were reconstructed only with 5 iterations.

Volume of Interest (VOI) Definition

All the reconstructed phantom images were processed and then analysed according to the protocol commonly adopted on patient data:

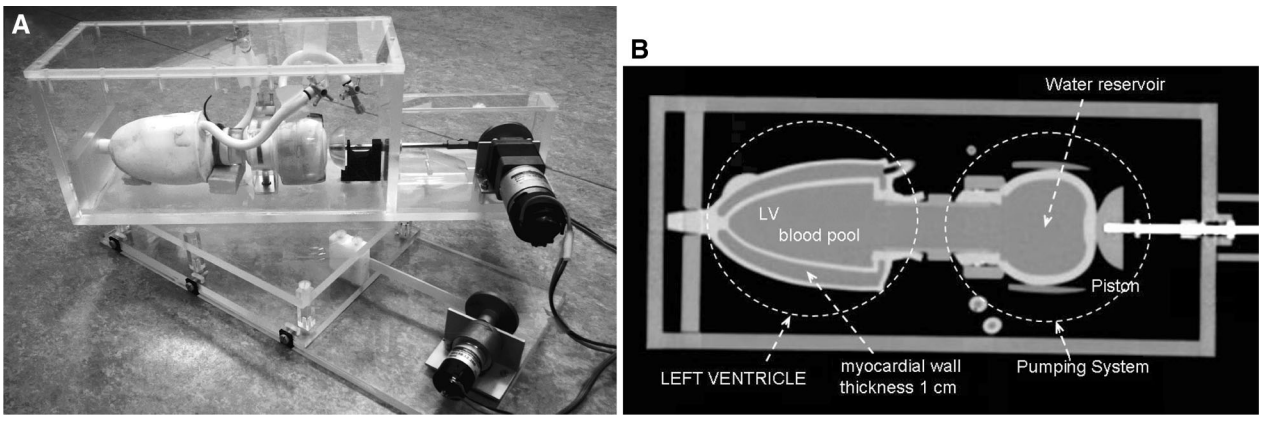

Figure 2. (**A**) A picture of the moving phantom, on the respiratory motion platform, showing the whole structures and the motors. (**B**) A CT image showing the internal structure of the phantom.

(1) Re-orientation of the LV along its short and long axes.[26]
(2) Definition of a VOI in the LV to simulate the sampling of the blood activity for Image-Derived-Input-Function (IDIF).
(3) Definition of the myocardial VOI. The myocardial wall was segmented in re-oriented short-axis images by means of an elliptical model. The phantom was divided in 23 slices along the long axis; the first 8 were considered ''apical'' the others ''mid'' or ''basal.'' In the apical slices, a spherical sampling was performed, using as a centre the ellipsoidal model previously extracted. An increasing number of points along the polar coordinate was taken, as the azimuthal coordinate increased (from N = 1 to N = 30). For more basal slices, a polar sampling was performed in each slice, using 36 samples per slice (one every 10°). To partially reduce noise each point was dilated to its four in-plane nearest neighbours. This procedure was performed on the averaged image of the longest frames, with some additional post-smoothing applied. Given the phantom dimensions, it means that each sampling point is farther than 4 mm from any other two adjacent points.

Metrics Used for Performances Evaluation

The following metrics were used to quantify the algorithms performances in the different VOIs.

Hot areas (i.e., LV, myocardium in the second experiment)

(1) Ratio between activity measured in VOI and true activity (a/a_{true})
(2) Ratio between STD of the activity measured in VOI among different noise realisations and true activity (STD(a))/a_{true})

For cold areas (i.e., defects in the second experimental configuration, myocardium in the first one), metrics were modified, with the use of a suitable reference, lacking the true activity:

(1) Cold contrast (a/a_{REF})
(2) Ratio between STD of the activity measured between different noise realisations and activity in the reference (STD(a))/a_{REF})

RV was used as a reference in the first experimental configuration because it was the hottest structure in the phantom and also a source of spill-in for the myocardium. Myocardium was used as a reference for the two defects.

RESULTS

Static Phantom, First Configuration: Bolus Passage

LV region (high activity—large dimension—low PVE). All the algorithms estimated correctly the activity in LV (within ±1.5%) for all the frame lengths. In Figure 3, the STD of the LV activity among different noise realisations is shown for 10 seconds frames. STD is generally lower than 3% of the true LV activity. The inclusion of the TOF information in the reconstruction process, allowing for a more accurate localization of the activity distribution, clearly reduces the variability of the estimated activity, always below the values provided by analytical algorithms. Conversely, the effect of the PSF recovery in a region scarcely affected by PVE is an increase of the variability with iterations. Results for the other frame length are comparable, with the STD contained in a range between 4%-6% for the 2 seconds frames and 0.3%-0.8% for 40 seconds frames.

Myocardium region (no activity—small dimension—high PVE). The activity measured in the myocardium showed variations depending on the algorithm as well as on the frame length (Figure 4A, B). Iterative algorithms showed an increase of the estimated activity (bias) with decreasing frame length (Figure 4A), while analytical algorithms showed a nearly constant value (about 3% and 3.3% of the RV activity for TOF-FBP and RP, respectively). Both TOF and PSF contributed to a better cold contrast, leading the algorithm TOFPSF with 5 or more iterations to the best results. Inclusion of TOF seems the most effective, since all the algorithm accounting for it behave well. The PSF modelling contributes by compensating for the PVE due to the activity spill-in from the two ventricles. However, its convergence is slow and thus the effect becomes evident only with more iterations (Figure 4A). It should be noted (Figure 4B) that the inclusion of PSF

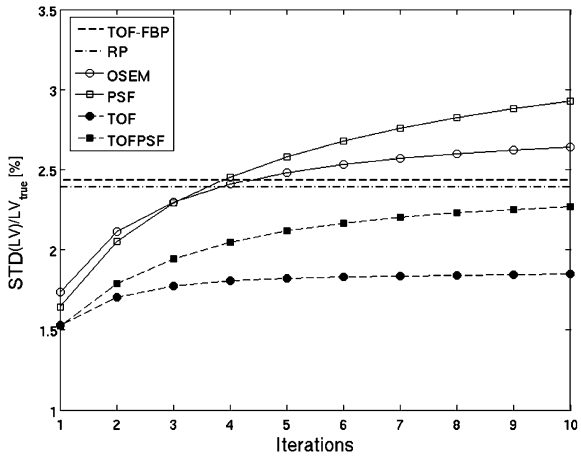

Figure 3. Standard deviation among the noise realisations of the activity measured in the LV. The frame length was 10 seconds. In this and all the following graphs, when the x axis shows the number of iterations, the analytical algorithms are depicted as an *horizontal line* for easier visual comparison.

modelling reduces markedly the dependence of the convergence value with frame length. Nonetheless, the difference between the convergence value of all iterative algorithms was small in the frame lengths investigated. TOFPSF had the lowest variation from 2.6% at 40 seconds to 3.2% at 2 seconds. TOF, PSF and OSEM showed variations from 3.2% to 5%, 4.5% to 5% and 5% to 6.6%, respectively.

The STD between the noise realisations was lower than 0.1% of the RV activity for all the iterative algorithms at 10 seconds frame length. Analytical algorithms showed higher variations: 0.35% (TOF-FBP) and 0.6% (RP).

Static Phantom, Second Configuration: Steady State

Representative reconstructed images for two count statistics are shown in Figure 5.

Myocardium region (high activity—small dimension—high PVE). Results in Figure 6 refer to the 15 seconds frames. The myocardial activity was found to be nearly completely recovered, after 5 iterations, by the iterative algorithms accounting for PSF (PSF and TOFPSF) (Figure 6A). This clearly shows that for a hot target with dimension of 1 cm as the myocardium the PSF modelling is effective in recovering PVE. Conversely, iterative and analytic algorithms not accounting for the PSF underestimated the true activity of about 15% and 10%, respectively. The introduction of TOF information in iterative algorithms appears to increase the convergence rate. Algorithms performances were equivalent at other frame lengths.

About the STD of the global myocardial VOI among the multiple noise realisations (Figure 6B), again the PSF modelling succeeded in providing the best results. A possible explanation is that the PVE correction improves the activity distribution uniformity in the myocardium, which is contaminated by the activity (spill-in) of LV, RV and mediastinum regions. The best results are obtained with PSF and by TOFPSF. However, it is worth noticing the tendency of the PSF and TOFPSF curve to further increase after 10 iterations. TOF alone was consistently better than OSEM and, in this case, comparable with the analytic algorithms after 5 iterations.

Defects (no activity—small dimension—high PVE). Images corresponding to a slice where both the defects can be seen are shown in Figure 7.

Results obtained in the two cold defects closely resemble those found in the cold myocardium in the first configuration of this phantom. The activity measured in the defects decreases with the iteration number. Both PSF and TOF contribute to reduce the activity and the best results are obtained with TOFPSF. The action of PSF is in this case more relevant than that of TOF, due to the small size of the defect. TOF, however, speeds up convergence.

Even in this case no particular dependence on the frame length was noticed. The STD between the noise realisations was the smallest with TOFPSF. TOF-FBP showed results comparable to the iterative algorithms (Figure 8) while RP algorithm had the highest noise confirming that in cold regions analytic algorithms have poor noise performances.

A summary of the results obtained in the two static phantom configurations is reported in Table 1.

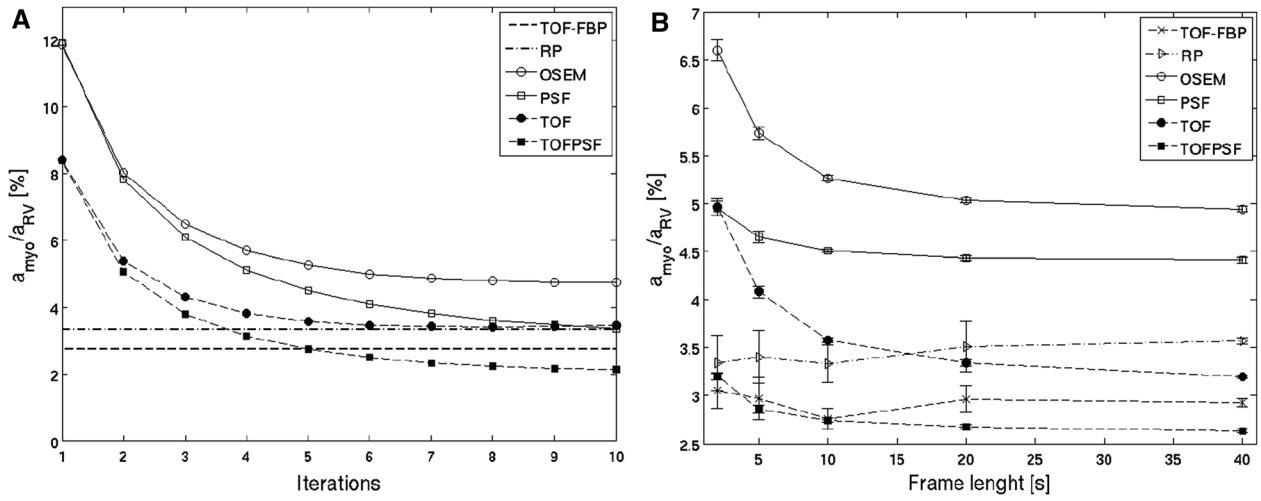

Figure 4. (**A**) Activity as a function of the iterations for the 10 seconds frames; (**B**) activity measured in the myocardium, as a function of frame length. For the iterative algorithms at 5 iterations.

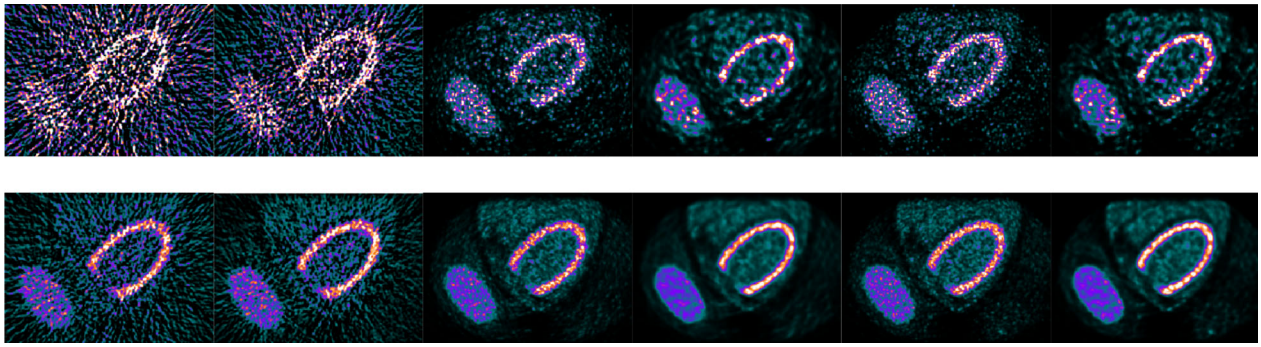

Figure 5. Example of reconstructed images from the second configuration (steady state) of the static phantom. *Upper row* 5 seconds acquisitions. *Lower row* 45 seconds acquisitions. All the iterative reconstructions are shown at 5 iterations. *Left to right* RP, TOF-FBP, OSEM, PSF, TOF and TOFPSF. The same window levels are used for all images.

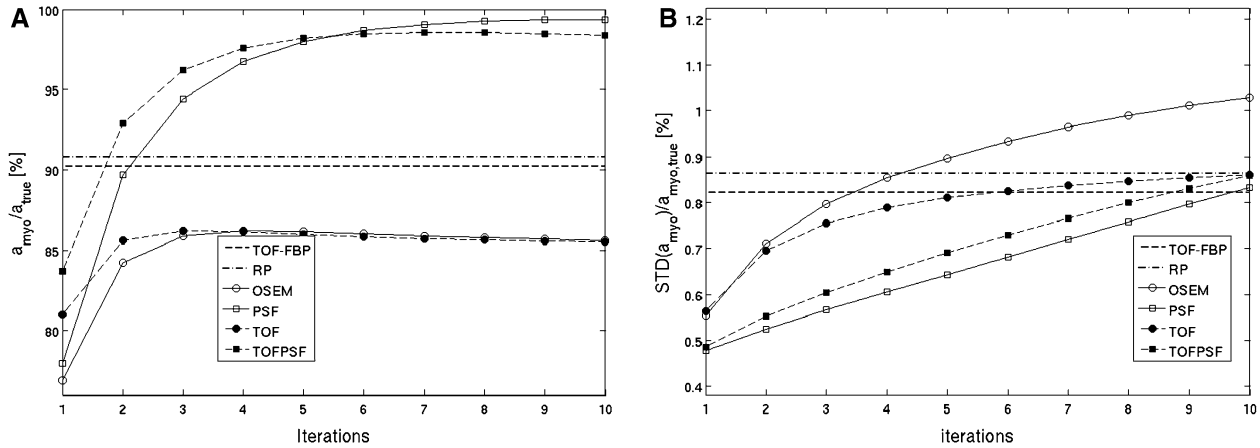

Figure 6. (**A**) Activity in the myocardium as a function of the iterations; (**B**) STD amongst the different noise realisations of the myocardial activity. Data refer to 15 seconds frames.

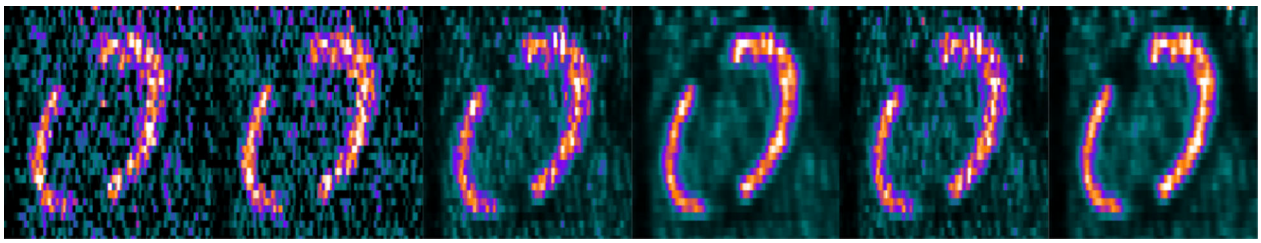

Figure 7. Example of reconstructed images (coronal slices) from the second configuration showing the two defects (45 seconds acquisitions, iterative reconstructions shown at 5 iterations). *Left to right* RP, TOF-FBP, OSEM, PSF, TOF and TOFPSF. The same window levels are used for all images.

Selection of the Number of Iterations

Based on the results obtained in the previous experiments, 5 iterations were identified as a good quantitative, qualitative and computational compromise for the reconstruction of clinical data, in particular for TOFPSF algorithm. The combination of TOF and PSF in fact provides generally the best results (quantitative and qualitative) when all the possible situations (hot and cold) commonly encountered in cardiac perfusion studies are considered. From the computational standpoint, the time needed for the reconstruction of 1 iteration using the dedicated computing system of the scanner is

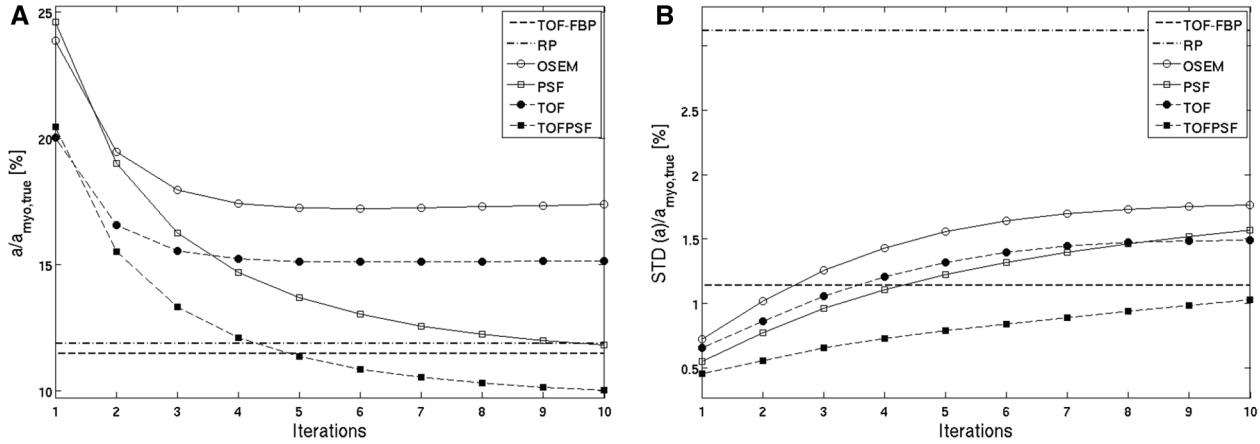

Figure 8. (**A**) Activity in the mid-anterior defect, as a function of the iterations; (**B**) STD of the activity in the same defect as a function of the iterations. Data refer to 15 seconds frames.

Table 1. Summary of the results obtained in the two experiments using the static thorax/heart phantom

	First configuration				
	LV: High activity—large dimension—low PVE		Myocardium: No activity—small dimension—high PVE		
	Activity estimation	Noise	Activity estimation	Noise	Consistency vs frame length
Performance ranking	Similar	(1) TOF (2) TOFPSF (3) RP, TOF-FBP (4) OSEM (5) PSF (see Fig. 3)	(1) TOFPSF (2) TOF-FBP (3) TOF, RP (4) PSF (5) OSEM (see Fig. 4)	(1) Iteratives (OSEM, TOF, PSF, TOFPSF) (2) TOF-FBP (3) RP (see text)	(1) TOF-FBP, RP (2) PSF, TOFPSF (3) TOF, OSEM (see Fig. 4)
	Second configuration				
	Myocardium: High activity—small dimension—high PVE		Defects: No activity—small dimension—high PVE		
	Activity estimation	Noise	Activity estimation	Noise	
Performance ranking	(1) TOFPSF, PSF (2) RP, TOF-FBP (3) OSEM, TOF (see Fig. 6)	(1) PSF, TOFPSF (2) TOF, RP TOF-FBP (3) OSEM (see Fig. 6)	(1) TOFPSF (2) TOF-FBP, RP (3) PSF (4) TOF (5) OSEM (see Fig. 8)	(1) TOFPSF (2) TOF-FBP (3) PSF, TOF (4) OSEM (5) RP (see Fig. 8)	

The algorithms were ranked from the best (1) to the worst (5) performance, those with similar performance were given the same ranking.

of about 1 minute, therefore the reconstruction of a typical 20 frames dynamic study with 5 iterations each require about 1 hour and a half. Five iterations were thus used in the third experiment.

Moving Phantom: Static Condition

The results obtained with the phantom in the static condition confirmed those found in the previous experiments. When the LV was the hottest area, as in the first configuration, its activity was correctly quantified. When it was cold, the relative performance of the algorithms, in regard to the myocardial wall, agreed with the second configuration. Analytical algorithms showed a clear trend between the recovered activity ratio (a/a_{true}) in the myocardium and the true contrast. In fact, with RP and TOF-FBP the measured activity in the myocardium increased from 80% (LV:myocardium < 1:5), up to 95% when the ratio was reversed (LV:myocardium > 5:1), Figure 9. A similar trend was seen also with OSEM, but it was less pronounced. Other algorithms did not show such trends. Regarding the measured activity in the LV, a greater range of variation across the different contrast levels was seen for all algorithms. In particular, when the LV was the hottest structure, it was correctly quantified, while as the myocardium became hotter, its activity was increasingly overestimated. In particular, with a 1:20 LV:myocardium activity ratio the LV activity was overestimated by about 3 times. In all cases, all algorithms proved to behave linearly, with the recovered activity being directly proportional to the true contrast.

Moving Phantom: Moving Condition

In the acquisitions with the phantom in motion, the quantification of the LV activity was similar to the static acquisition. It was correctly quantified when the LV was the hottest structure and then it was progressively overestimated as it became colder than the myocardium. The myocardium, instead, suffered appreciably from the influence of motion (Figure 9): when it was colder than the LV its activity was overestimated while, when it was the hottest structure, it was underestimated. In conditions of hot myocardium (e.g., LV:myocardium < 1:5) the activity was distinctly underestimated as compared to the second configuration of the static phantom and to the static acquisition of this one. In conditions of hot LV (e.g., LV:myocardium > 7:1) the myocardial activity was consistently overestimated, between 25% for TOF-PSF and 45% for RP. TOF performed similarly to TOF-FBP, RP and OSEM while PSF behaved similarly to TOFPSF. While the absolute performance of the reconstruction algorithms worsened compared to the previous studies, the effect of motion did not modify the relative performances of the different algorithms.

DISCUSSION

The quantification of MBF using 3D-PET, dynamic scans and kinetic modelling is an established diagnostic technique useful to evaluate coronary macro- and microcirculation. It allows the evaluation of global impairment of the hyperaemic response to stressors on top of the localization of regional under-perfusion. The accuracy and precision of the quantification by kinetic modelling, however, depends on the quality of the acquired data (i.e., scanner performances) and of the corresponding reconstructed images. This is especially important in cardiac dynamic perfusion studies, where a number of critical conditions are met, like very high count rates as well as the need to sample very short-time intervals. Reconstruction algorithms have the possibility to improve image accuracy by means of a correct modelling of the statistics of photon coincidences collection, a more precise correction for physical effects (scatter, randoms) and the recent possibility to include TOF information and PSF modelling in the reconstruction scheme. For this reason, we investigated the features of different reconstruction algorithms (analytic and iterative) that exploit all these innovations. The parameters of the reconstruction algorithms investigated were set to achieve the best quantitative performances and not the best image quality (i.e., ramp filters for the analytic algorithms, very small post-filtering for iterative techniques, high number of iterations, etc.).

Three experiments were performed with the aim to cover the most representative conditions commonly found in clinical cardiac perfusion studies, after a careful matching of the limiting factors found in patient studies. In particular, the activity values used in the different experiments and in the different compartments of the phantoms were established from average patient uptakes.

Attenuation correction was also carefully applied accounting for the static and the motion condition of the two phantoms used in this work. In fact, a typical problem of cardiac studies is related to the motion of the heart that might lead to misalignments between the transmission (CT) and the emission (PET) data. If an helical CT is used, like for oncology studies, artifactual defects in the myocardial wall can be found in about 40% of the patients.[27] The use of a cine-CT has been shown to be effective in applications where respiratory motion was involved.[23] In the particular case of cardiac studies, the use of cine-CT has been shown to be a robust solution to the problem of mismatch.[22,27] Averaging techniques for attenuation correction are, in fact,

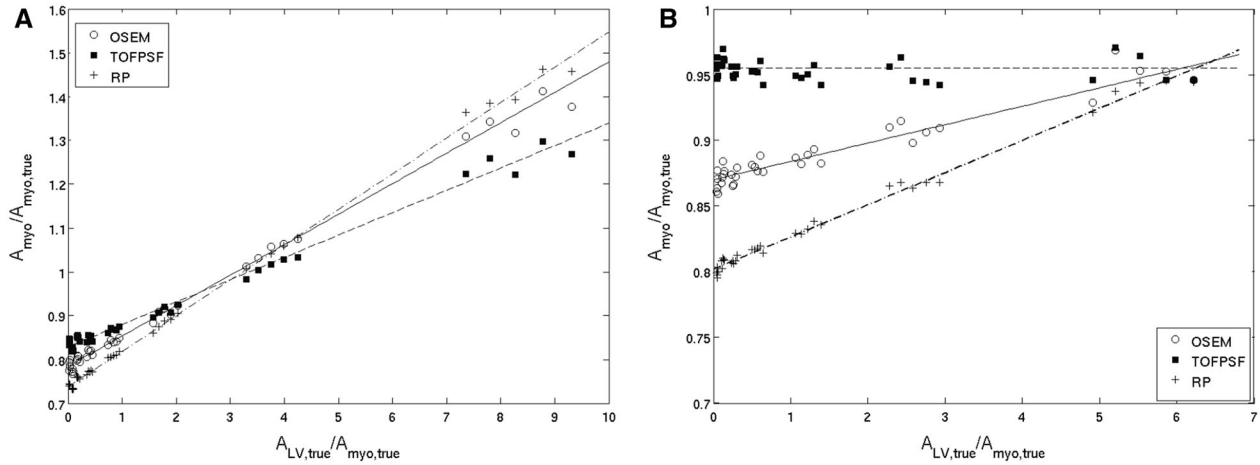

Figure 9. Ratio between the measured and the true activity in the myocardium as a function of the true activity ratio (contrast) between LV and myocardium. Only three algorithms are shown for clarity. *Left* (**A**) phantom in motion. *Right* (**B**) static acquisition.

suggested by the SNMMI/ASNC/SCCT guidelines for cardiac PET/CT.[28] This practice has the disadvantage of an higher dose, compared to helical CT. However, such increase can be limited, with proper optimization. Furthermore, well-matched PET and CT data can solve diagnostic ambiguities that arise as results of an incorrect attenuation correction.

Of the three experiments performed in this work, the first one simulated the passage of the tracer bolus in the heart. Its aim was to evaluate the accuracy in the quantification of the LV activity and its STD over repeated realisations that are important for the estimation of the IF. The IF value at the beginning of the scan is one of the two factors that impacts most the MBF quantification (the other being the myocardial activity in later frames). Its underestimation results in a proportional overestimation of the MBF and vice versa. Furthermore, since most of the activity is concentrated in only 2 frames, it is especially important to have as low noise as possible. The results obtained showed that the measured activity in the LV was correctly estimated at the statistics (frame lengths) here considered by all the algorithms. From the variability point of view, TOF gave the best results in terms of noise reduction. A second target of this experiment was the assessment of the eventual positive bias present in IRs in the cold myocardium region. The results highlighted that it was present, however, that its magnitude was very limited, even in case of frames as short as 2 seconds. It was found that PSF further reduced the amount of bias, similarly with what was found in the field of neurology.[13] On top of this, TOF improved cold contrast at all iterations. PSF also improved results, but it needed more iterations. Analytical algorithms did not show any trend with statistics and performed as well as TOF and TOFPSF in terms of cold contrast. However, the analysis of the noise realisations showed that they had higher levels of noise.

The second configuration, complementary to the previous one, was representative of the steady state when the activity is accumulated in the myocardial tissue. Furthermore, two defects were simulated in the myocardium to evaluate the performances of the algorithms in infarcted regions. The main objective was to evaluate the accuracy in the quantification of the myocardial activity, and the associated noise levels. An underestimation of myocardial activity reflects in a proportional underestimation of the MBF, while the noise in the myocardial activity directly affects the statistical error on the fitted MBF. As expected, PSF showed the best performance in the estimation of the myocardial activity, by recovering PVE. In this case, the action of TOF was less effective than in the first experiment, but it still helped in speeding up convergence. Analytical algorithms performed slightly better than OSEM and TOF, but their performances did not match those of PSF. The recovery of the myocardial activity given by PSF, of about 15%, is expected to be translate in a proportional increase of the fitted MBF. This is in accordance with the results published by Armstrong et al,[17] that reported an increase of about $\sim$10% in the fitted MBF when using TOFPSF reconstruction, compared to standard OSEM. The noise in the myocardium, quantified as the STD between the noise realisations, was minimised by PSF and TOFPSF, within the 10 iterations considered in the work. The positive impact of the combined action of TOF and PSF was even more prominent in the evaluation of the two

simulated defects. TOF improved cold contrast at all iterations, while PSF, as in the case of cold myocardium region, improved the performances, by reducing PVE, but only after more iterations (>5). In fact, in cold regions convergence is slower than in high activity regions, thus more iterations should be used to achieve the best results. In the defects, the STD between the noise realisations was markedly higher for RP than for all other algorithms.

Finally, a dynamic-moving phantom simulating the left ventricle was used to assess the performances of the different reconstruction algorithms over a wide range of activity ratios between LV and myocardium and whether the motion (cardiac and respiratory) could change the findings obtained in static conditions. Motion worsened myocardial activity recovery, nonetheless all the algorithms maintained consistent performances with that obtained in the static experiments. In particular, movement induced an underestimation of the myocardial activity when the myocardium was hotter than the surrounding (i.e., LV) and an overestimation, when the situation reversed. TOFPSF still provided the most correct activity values. It was also determined that the relation between the measured to true activity ratio and the myocardium to LV contrast was linear in the whole investigated range. This finding is particularly important because it justifies the partial volume correction algorithm implemented in most software programs for kinetic modelling. These strategies, in fact, model the activity measured in the myocardium as a linear mixture of true myocardial activity and LV activity,[29] and fit the mixing parameter to the measured data.

The results obtained in this work are expected to be applicable to most cardiac quantitative studies, independently from the tracer used, whether in perfusion studies (e.g., ^{15}O-water, ^{13}N-ammonia) or metabolic tracers studies, like ^{18}F-FDG or ^{11}C-acetate. However, the applicability might be limited for ^{82}Rb, since this nuclide has a much larger positron range, impacting PSF modelling. A limitation of this study is that all the experiments and reconstructions have been performed using the Discovery-690 GEMS scanner (hardware and software), thus the results cannot be directly generalised to other PET/CT systems. Nonetheless, we believe that state of the art PET systems with comparable physical performances and similar implementation of the reconstruction algorithms should give similar results, as generally seen when comparing different algorithms like OSEM, TOF and PSF implemented on different scanners for oncological applications.

NEW KNOWLEDGE GAINED

The behaviour of different image reconstruction algorithms (analytic and iterative) in condition of high and low statistics was determined and they all were found to be reliable. The amount of bias introduced by the IR algorithms was determined and found to be limited, even for frames significantly shorter than the ones usually adopted in clinics. Iterative algorithms including TOF and PSF modelling were found to outperform the others, in terms of: (i) activity estimation for hot and cold targets, and (ii) variability of the results (STD of the noise realisations).

CONCLUSIONS

IR (OSEM) accounting for TOF and PSF can be recommended for the quantification of dynamic cardiac PET studies as they improve the results compared to analytics and standard OSEM.

Disclosure

All the authors have nothing to disclose.

APPENDIX

The Reconstruction Algorithms

All the iterative algorithms used in this work were provided by the scanner manufacturer. They are all based on a 3D-OSEM algorithm, with all the relevant corrections implemented in the iterative scheme as

$$I_n^{i+1} = \frac{I_n^i}{\sum_m H_{m,n} M_m} \sum_m \frac{H_{m,n} M_m P_m}{M_n \sum_{n'} H_{m,n'} I_{n'}^i + A_m},$$

where I_n^{i+1} and I_n^i are the values of the nth image pixel of the images I at the ith + 1 and ith iteration. P_m is the mth sinogram element, M_m is a matrix accounting for all the multiplicative correction to be applied to the mth sinogram element (normalisation, dead-time and attenuation) and A is the matrix of the additive corrections accounting for random and scatter coincidences. The matrix H account for the system geometry, which represent the probability for a photon emitted from the nth image pixel to be recorded in the mth projection bin.

The PSF modelling is achieved by modifying the H operator to H' such that $H'_{m,n} = \sum_k D_{m,k} H_{k,n}$, where D represents the detector response model. Note that the PSF has been implemented as a spatially variant model in the sinogram domain.

The iterative algorithms, including TOF, have a basic implementation, like the OSEM counterpart, but the events are weighted according to the TOF probability distribution by a TOF kernel T, which estimates the contribution from each voxel n, to the time bin t of the projection bin m considered

$$I_n^{i+1} = \frac{I_n^i}{\sum_{m,t} H_{m,n} M_m T_{n,t}} \sum_{m,t} \frac{H_{m,n} M_m P_m T_{n,t}}{M_n \sum_{n'} H_{m,n'} T_{n',t} I_{n'}^i + A_{m,t}}.$$

The multiplicative corrections and the PSF implementation work as in the non-TOF case while the additive correction requires TOF to be taken into consideration (i.e., the random coincidences are split equally between each time bin, while the scatter distribution is time dependent).

Scatter coincidences are iteratively estimated using a 3D model-based scatter simulation[30] that computes the fraction of the single scatter, following a convolution procedure is used to estimate multiple scatter, finally scaling the results to the emission tails. For TOF reconstruction, the same procedure is used but the simulation account for the distribution along the temporal dimension. Random coincidences are estimated from detectors single count rates.

The RP algorithm we used was also provided by the scanner vendor. The filters were based on what described by Kinahan and Rogers.[5] Scatter and random coincidences were estimated with the same algorithms as for OSEM and, subsequently, subtracted from the sinogram.

The TOF-FORE-FBP algorithm was implemented off-line by our group using a research-tool software provided under a research collaboration with GEMS which uses the same routines as in the PET scanner. The implementation it is based on the work by Defrise et al[24] for the TOF implementation of FORE and the TOF-FBP procedure uses the same filter described by Conti et al[25] to reconstruct the rebinned 2D-TOF sinograms. Scatter coincidences were simulated in the same way of the TOF iterative algorithms in 3D. Once estimated, scatter and random coincidences were subtracted from the 3D-TOF sinograms. Subsequently, the sinogram was corrected for detector geometry, dead-time, normalisation and attenuation. Finally, the 3D data were rebinned to 2D using FORE, before the TOF-FBP reconstruction.

References

1. Herzog BA, Husmann L, Valenta I, Gaemperli O, Siegrist PT, Tay FM, et al. Long-term prognostic value of 13N-ammonia myocardial perfusion positron emission tomography added value of coronary flow reserve. JACC 2009;54:150-6.
2. Fiechter M, Ghadri JR, Gebhard C, Fuchs TA, Pazhenkottil AP, Nkoulou RN, et al. Diagnostic value of 13N-ammonia myocardial perfusion PET: Added value of myocardial flow reserve. J Nucl Med 2012;53:1230-4.
3. DeGrado TR, Bergmann SR, Ng CK, Raffel DM. Tracer kinetic modeling in nuclear cardiology. J Nucl Med 2000;7:686-700.
4. Yu M, Nekolla SG, Schwaiger M, Robinson SP. The next generation of cardiac positron emission tomography imaging agents: Discovery of flurpiridaz F-18 for detection of coronary disease. Semin Nucl Med 2011;41:305-13.
5. Kinahan PE, Rogers JG. Analytic 3D image reconstruction using all detected events. IEEE Trans Nucl Sci 1989;36:964-8.
6. Søndergaard HM, Madsen MM, Boisen K, Bøttcher M, Schmitz O, Nielsen TT, et al. Evaluation of iterative reconstruction (OSEM) versus filtered back-projection for the assessment of myocardial glucose uptake and myocardial perfusion using dynamic PET. Eur J Nucl Med 2007;34:320-9.
7. Visvikis D, Griffiths D, Costa DC, Bomanji J, Ell PJ. Clinical evaluation of 2D versus 3D whole-body PET image quality using a dedicated BGO PET scanner. Eur J Nucl Med 2005;32:1050-6.
8. Riddell C, Carson RE, Carrasquillo JA, Libutti SK, Danforth DN, Whatley M. Noise reduction in oncology FDG PET images by iterative reconstruction: A quantitative assessment. J Nucl Med 2001;42:1316-23.
9. Wang CX, Snyder WE, Bilbro G, Santago P. Performance evaluation of filtered backprojection reconstruction and iterative reconstruction methods for PET images. Comput Biol Med 1998;28:13-24.
10. Reilhac A, Tomeï S, Buvat I, Michel C, Keheren F, Costes F. Simulation-based evaluation of OSEM iterative reconstruction methods in dynamic brain PET studies. Neuroimage 2008;39:359-68.
11. Walker MD, Asselin MC, Julyan PJ, Feldmann M, Talbot PS, Jones T, et al. Bias in iterative reconstruction of low-statistics PET data: Benefits of a resolution model. Phys Med Biol 2011;56:931.
12. Conti M. Focus on time-of-flight PET: The benefits of improved time resolution. Eur J Nucl Med 2011;38:1147-57.
13. Karp JS, Surti S, Daube-Witherspoon ME, Muehllehner G. Benefit of time-of-flight in PET: Experimental and clinical results. J Nucl Med 2008;49:462-70.
14. Conti M. Why is TOF PET reconstruction a more robust method in the presence of inconsistent data? Phys Med Biol 2011;56:155.
15. Bettinardi V, Castiglioni I, De Bernardi E, Gilardi MC. PET quantification: Strategies for partial volume correction. Clin Transl Imaging 2014;2:199-218.
16. Le-Meunier L, Slomka PJ, Dey D, Ramesh A, Thomson LE, Hayes S, et al. Enhanced definition PET for cardiac imaging. J Nucl Cardiol 2010;17:414-26.
17. Armstrong IS, Tonge CM, Arumugam P. Impact of Point Spread Function modeling and time-of-flight on myocardial blood flow and myocardial flow reserve measurements for rubidium-82 cardiac PET. J Nucl Cardiol 2014;21:1-8.
18. Bettinardi V, Presotto L, Rapisarda E, Picchio M, Gianolli L, Gilardi MC. Physical performance of the new hybrid PET/CT discovery-690. Med Phys 2011;38:5394-411.
19. M Iatrou, SG Ross, RM Manjeshwar, CW Stearns, A fully 3D iterative image reconstruction algorithm incorporating data corrections. In: IEEE Nuclear Science Symposium Conference Record, vol. 4, p. 2493-2497.
20. Alessio AM, Stearns CW, Tong S, Ross SG, Kohlmyer S, Ganin A, Kinahan PE. Application and evaluation of a measured spatially variant system model for PET image reconstruction. IEEE Trans Med Imaging. 2010;29:938-49.
21. Presotto L, Bettinardi V, Petta P, Gilardi MC. A compact dynamic phantom to assess the effect of motion in cardiac PET and SPECT studies. In: Nuclear Science Symposium and Medical Imaging Conference (NSS/MIC), 2012 IEEE, p. 2638, 2642; 2012.
22. Alessio AM, Kohlmyer S, Branch K, Chen G, Caldwell J, Kinahan P. Cine CT for Attenuation Correction in Cardiac PET/CT. J Nucl Med 2007;48:794-801.
23. Cheng NM, Yu CT, Ho KC, Wu YC, Liu YC, Wang CW, et al. Respiration-averaged CT for attenuation correction in non-small-cell lung cancer. Eur J Nucl Med Mol Imaging 2009;36:607-15.

24. Defrise M, Casey ME, Michel C, Conti M. Fourier rebinning of time-of-flight PET data. Phys Med Biol 2005;50:2749.
25. Conti M, Bendriem B, Casey M, Chen M, Kehren F, Michel C, Panin V. First experimental results of time-of-flight reconstruction on an LSO PET scanner. Phys Med Biol 2005;50:4507.
26. Cerqueira MD, Weissman NJ, Dilsizian V, Jacobs AK, Kaul S, Laskey WK, et al. Standardized myocardial segmentation and nomenclature for tomographic imaging of the heart. Circulation 2002;105:539-42.
27. Gould KL, Pan T, Loghin C, Johnson NP, Guha A, Sdringola S. Frequent diagnostic errors in cardiac PET/CT due to misregistration of CT attenuation and emission PET images: A definitive analysis of causes, consequences, and corrections. J Nucl Med 2007;48:1112-21.
28. Dorbala S, Di Carli MF, Delbeke D, Abbara S, DePuey EG, Dilsizian V, et al. SNMMI/ASNC/SCCT guideline for cardiac SPECT/CT and PET/CT 1.0. J Nucl Med 2013;54:1485-507.
29. Hutchins GD, Caraher JM, Raylman RR. A region of interest strategy for minimizing resolution distortions in quantitative myocardial PET studies. J Nucl Med 1992;33:1243-50.
30. Polycarpou I, Thielemans K, Manjeshwar R, Aguiar P, Marsden PK, Tsoumpas C. Comparative evaluation of scatter correction in 3D PET using different scatter-level approximations. Ann Nucl Med 2011;25:643-9.